AUSTENITIC STAINLESS STEEL AND MARTENSITIC TRANSFORMATION IN WELDED HIGH-HARDNESS ARMOR STEEL

UDC:621.791:669.018.25
Original scientific paper https://doi.org/10.46793/adeletters.2023.2.2.4

Aleksandar Čabrilo[1*], Nenad Janjić[1], Vladimir Blanuša[1], Miloš Jovanović[2]

[1]The Higher Education Technical School of Professional Studies, Novi Sad, Serbia
[2]Welding Institute, Ljubljana, Slovenia

Abstract:
An austenitic filler material is traditionally used for welding armor steels, thus avoiding the negative effect of hydrogen content due to slow diffusion towards the sensitive fusion line. For heavy structural engineering such as armored military vehicles, which are frequently affected by impact and dynamic load, it is crucial to know the dynamic properties of the most sensitive area of welded joints, the weld metal zone. Due to a significant interest in quantifying material resistance to crack initiation and propagation, the fatigue crack growth rate was measured in the welded metal zone, while the resistance to crack growth in the weld metal was tested by the amount of austenite transformed into martensite. Accordingly, the threshold stress concentration factor was 10 MPa $m^{1/2}$. XRD spectral analysis revealed a direct transformation of γ - austenite into α'-martensite.

ARTICLE HISTORY
Received: 26 December 2022
Revised: 5 April 2023
Accepted: 17 May 2023
Published: 30 June 2023

KEYWORDS
Armor steel, fatigue crack growth, austenitic stainless steel, austenitic filler material, martensitic transformation, welding, armored military vehicles

1. INTRODUCTION

The austenitic filler material is traditionally used for armor steel welding because hydrogen dilution improves in an austenitic phase [1]. This avoids adverse hydrogen content effects, such as slow diffusion towards the sensitive fusion line and crack formation [2]. After the welding process, solidification cracking may result from high thermal expansion of the austenitic stainless steel [3], and invisible defects may be created in the weld metal zone [4].

Due to variable loads, cracks in the weld metal may easily propagate towards the sensitive fusion line, followed by their possible rapid growth [5]. The presence of delta ferrite reduces ductility and potential toughness. In addition, austenite/ferrite boundaries could be preferential sites for the precipitation of $M_{23}C_6$ type carbides [6].

Although austenitic filler material is used the most frequently for welding and has several unusual features, including its high manganese content, few articles consider the problem of its mechanical properties. There are numerous studies of fatigue crack growth in austenitic materials, but mainly due to deformation, with only a few investigating austenitic weld metals [7]. The austenitic filler material is unstable and transforms into martensite during fatigue crack propagation due to plastic deformation at the crack tip [8]. During the metastable austenite deformation, two types of martensitic structures can be formed: ε – martensite with hexagonal close-packed and α' – martensite, with a body-centered cubic crystal structure. Austenite into martensite transformation is related to the stacking fault energy. If the stacking fault energy is <20 J/m^2, transformation proceeds according to the model: γ → ε → α'. If it is larger, then the direct γ → α' transformation occurs [9]. It is known that manganese and nickel stabilize martensite and prevent martensitic transformation. It should be noted that an upper limit of stacking fault energy of austenite-martensite phase transition varies [10,

*CONTACT: Aleksandar Čabrilo, e-mail: cabrilo@vtsns.edu.rs

11]. An amount of austenite transformed into martensite is directly related to crack growth resistance in the weld metal [12].

X-ray diffraction investigated martensitic transformation effects on fatigue crack growth in the Paris region. Fracture surfaces for the impact energy and fatigue crack growth tests were also investigated by Scanning Electron Microscope (SEM).

2. MATERIALS AND METHODS

2.1 Materials and welding process

Gas metal arc welding (GMAW) and AWS ER307 solid wire are used for welding armor steel Protac 500. The welding direction is parallel to the rolling direction. Cold rolled plates 12 mm thick are cut to the required dimensions (250 x 100 mm), while V joint under the angle of 55° is prepared by Water Jet Device Fig. 1. Robot Kuka and Citronix 400A device was used during the welding process testing. Details on welding are shown in the article [13]. Robotic welding is used for human factor effect elimination to allow a fine adjustment of parameters and results repeatability. The wire diameter is 1.0 mm, while Fig. 1 shows V joint dimensions and four-pass welding configuration.

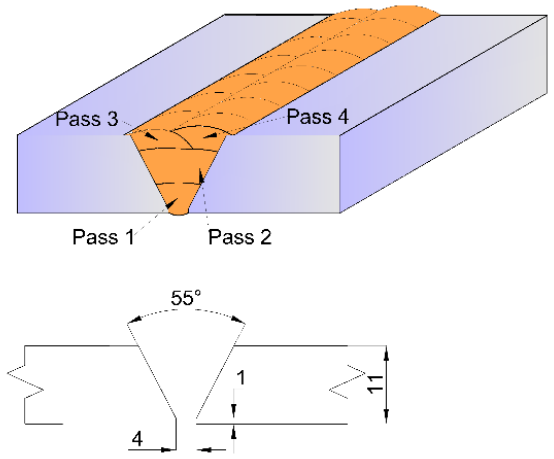

Fig. 1. Schematic representation of a welded joint and pass position

The base material chemical composition obtained by spectro-chemical analysis is shown in Table 1, while the filler material chemical composition is shown in Table 1. Spectro-chemical analysis was performed after the welding process.

Table 1. Chemical composition of the base and filler material [1]

Material	*Chemical composition [mass fraction %]*										
	C	***Si***	***Mn***	***S***	***Cr***	***P***	***Al***	***Cu***	***Ni***	***Mo***	***V***
Protac 500	0,27	1,07	0,71	0,001	0,64	0,009	0,054	0,28	1,094	0,296	0,039
ER307	0,08	0,89	6,29	0,001	17,8	0,014	0,01	0,08	8,24	0,13	0,03

2.2 Fatigue crack growth test

Three-point bending specimen, SEN (B), was used for testing [14]. The schematic drawing of specimen for fatigue crack growth test is shown in Fig. 2. Water Jet Device cut the specimens to eliminate any possibility of armor steel thermal treatment. After getting final measures in the grinding process, a 5 mm long machined notch was created on specimens in the direction parallel to welding Fig. 3, according to the E-647 standard [15]. The fatigue pre-crack was inserted before the crack growth rate tests, in accordance with ASTM E647 [15]. The length of the fatigue pre-crack was 4.7 mm. The fatigue pre-crack was realized with a high-frequency CRACTRONIC pulsator at a load ratio R = 0.33, followed by a constant loading frequency of 170 Hz. Fatigue crack growth rate was tested on a high-frequency CRACTRONIC pulsator, the model with force and frequency control of 145 Hz. The constant sinusoidal shape was used, while the testing was made under the load ratio $R=K_{min}/K_{max}=0.1$.

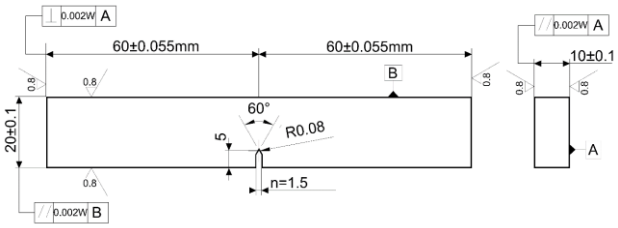

Fig. 2. Schematic drawing of the SEN (B) specimen with dimensions

The crack length was measured by RUMUL RMF A-10 measuring foils during the testing procedure. The number of cycles for each crack growth of 0.05 mm was automatically recorded in the experiments. Based on these records, the diagram

of ***a-N*** was drawn. ***a-N*** curves of dependence were used for crack growth rate ***da/dN*** determination.

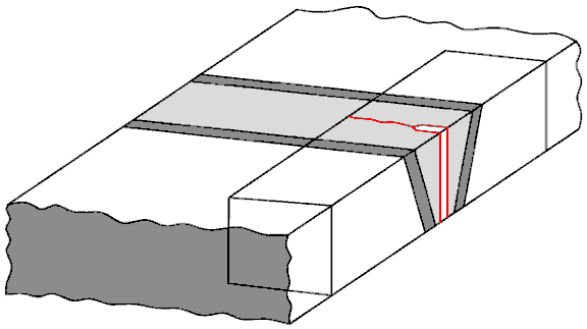

Fig. 3. Specimen orientation with respect to the weld axis for fatigue crack growth test

Three specimens were used for this test in the same testing conditions and initial loads. The result was an average value of three measurements. A fracture surface was analyzed by Scanning Electron Microscope JEOL JSM 6460LV at 25 kV.

3. RESULTS AND DISCUSSION

3.1 Fatigue crack growth behavior

Fig. 4 shows the crack growth rate in threshold region da/dN<10^{-4} mm/cycle. The threshold of stress concentration factor ΔK_{th} is 10 MPa $m^{1/2}$.

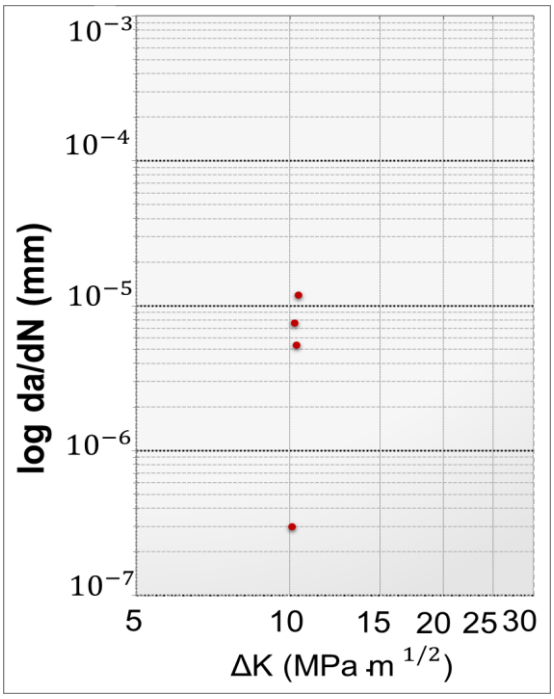

Fig. 4. Fatigue crack growth rate per cycle, da/dN, vs. stress intensity factor range, ΔK, in the near threshold region. Specimens pre-cracked in weld metal, tested at room temperature

The crack growth rate in the region of linear growth da/dN>10^{-4} mm/cycle is shown in Fig. 5. The constants C and m in this region amount to 4x10^{-11} and 5.3, respectively. The crack growth at the macro level is wavy and tortuous, Fig. 6.

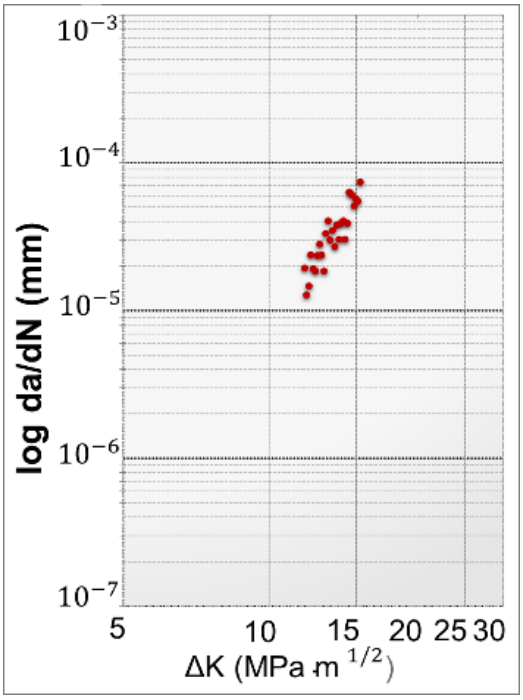

Fig. 5. Fatigue crack growth rate per cycle, da/dN, vs. stress intensity factor range, ΔK, in the linear region

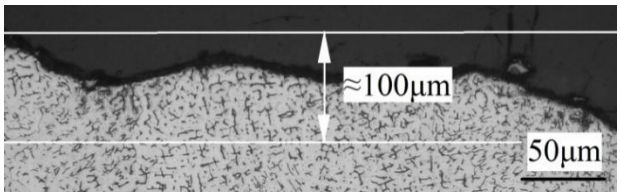

Fig. 6. Fatigue crack growth path in weld metal zone R=0.1. Crack growth direction is from left to right

3.2 Fatigue fractography analysis

Fig. 7 a) and b) show the fractography in the crack growth threshold region in the weld metal zone. The fatigue striations are visible on the fracture surface at 1 mm from the fatigue crack starting point and their size is about 3 μm.

Fig. 8 a) and b) show the linear crack growth area. The fatigue striations formed in this region are 4 to 5 times larger than in the threshold region and are up to 15 μm large.

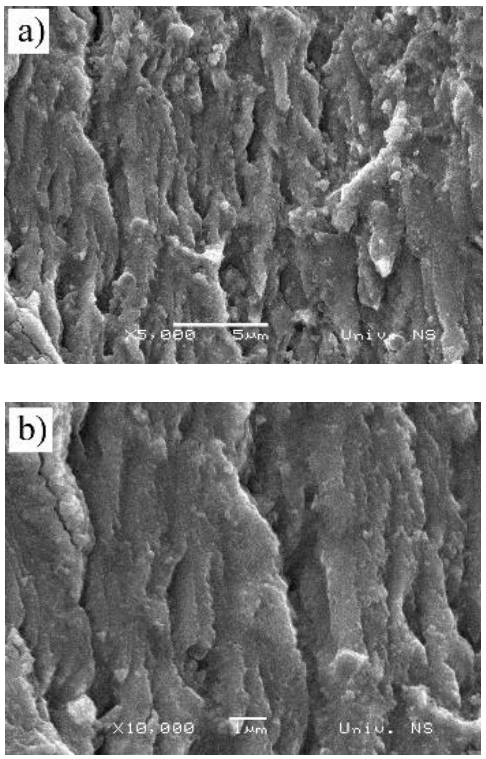

Fig. 7. SEM fractography at 1 mm from the fatigue crack starting point

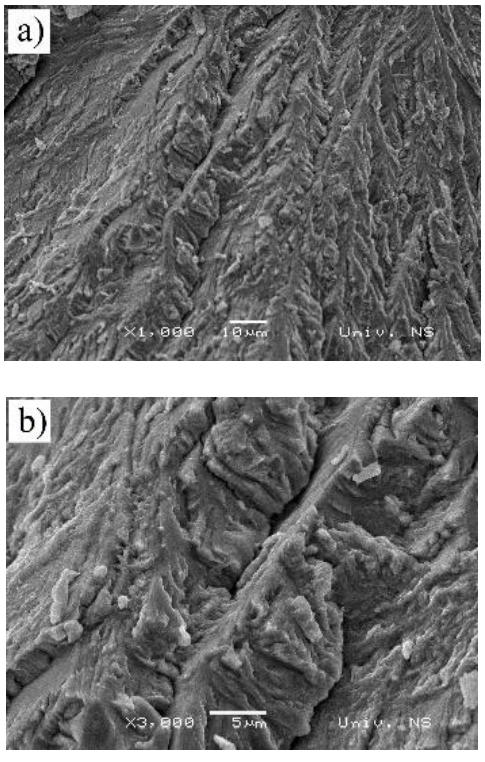

Fig. 8. Figure 15 SEM fractography at 6.5 mm from the fatigue crack starting point

3.3 XRD spectral analysis

Fig. 9 shows the X-ray diffraction results of the deformation-induced ***α´ martensite***. The changing amounts are shown per level concerning the fracture surface. The results show two phases, austenite and martensite. Both phases have two peaks, austenite with peaks of 2θ from 43.2-43.6 and 50.4-50.9, and martensite with its peaks at 43.5-44.2, 44.8 and 45.0.

Since higher surface roughness causes increased diffuse X-ray scattering, peak intensities inversely correlate with the thickness of the specimens under investigation. Nevertheless, using the RIR method (reference intensity ratio), the ratio of integrated intensities of **α´** martensite and austenite diffraction peaks reliably indicate their weight ratio in surface layers.

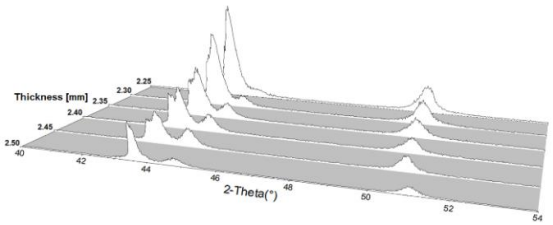

Fig. 9. XRD Diffractograms of specimens under investigation

The most intense peaks of α´ martensite and austenite overlap in our specimen and numerous alloys published in crystallographic databases [16]. The uncertainty inherent in heavily overlapping peaks deconvolution makes them unsuitable for weight ratio determination. Therefore, the second most intense peaks were used. These peaks are only twice less intense than their stronger counterparts and therefore are absolutely sufficient for precise weight ratio calculation.

Table 2 shows a change percentage per level concerning the fracture surface. α´ martensite was detected at distances up to 0.25 mm under the fracture surface. The greatest transformation of austenite into α´ martensite was 55%, seen on the fracture surface. In the depth perception tests, the amount of α´ martensite declines with a distance by an average of ≈5%/0.05 mm. At the distance of 0.25 mm, the amount of transformed austenite fell to 24%.

Table 2. ά - Martensite volume fractions vs. specimen thickness

	ά - Martensite volume fractions						
Specimen thickness	(mm)	2.50	2.45	2.4	2.35	2.30	2.25
ά -Martensite volume	(%)	55	50	46	34	30	24
Tolerance	(%)	±3	±3	±2	±2	±2	±2

The martensitic transformation took place due to plastic deformation at the crack tip. According to Von Mises criterion Eq. (1), the plastic zone radius in the linear growth region amounts to =0.14 mm.

$$r_{1p}^{*} = \frac{1}{4\pi}\left(\frac{K_I}{\sigma_T}\right)^2 \cdot \left(1 + \frac{3}{2}sin^2\theta + \cos\theta\right) \ (mm \qquad (1)$$

Schram and Reed [17] established a formula for stacking fault energy calculation, energy affecting a martensitic transformation possibility:

$$SFE = -53 + 6.2(\%Ni) + 0.7(\%Cr) + 3.2(\%Mn) + 9.3(\%Mo) \qquad (2)$$

The stacking fault energy for austenitic filler material is 32 mJ/m^2. This slightly higher stacking fault energy results from the higher manganese and nickel content in the austenitic filler material.

4. RESULTS AND DISCUSSIONS

Fatigue-induced fracture depends on external factors such as load and internal factors such as the mechanical properties of materials and microstructure. It is known that in stainless steel, being metastable materials, austenite transformation into martensite may occur during a fatigue crack growth, resulting from intensive plastic deformation at the crack tip. X-ray diffraction showed the direct transformation of austenite into α' martensite, which is typical for stainless steel with higher stacking fault energy. Martensitic transformation in these steels causes an increase in volume [18]. The resulting stress and strain fields that appear at the crack tip should be considered when determining the stress intensity factor [19]. Phase transformations at the crack tip [20] decrease the crack growth rate in the linear region [21]. Martensitic transformation occurs only in the thin layer close to the fracture surface. According to Eq. (1), the plastic zone in the region of linear growth has a radius of 0.14 mm, which matches the X-ray diffraction results, showing that the zone of intensive martensitic transformation is at a depth of 0.1 mm.

Based on the transformed martensite percentage, it can be noticed that crack growth is rather difficult. Delta ferrite in the austenitic base of the weld metal gives rise to crack deflection and spreading, thus decreasing the stress intensity factor at the crack tip; it reduces the crack growth rate in this region.

It is known that microstructural characteristics are significant for fatigue crack growth. Hence, the coefficient defining the crack growth in the Paris region has slightly higher values than usual. This can be explained by the multi-pass weld having a periodic hardened microstructure.

In this research, the crack growth was normally monitored concerning the growth direction of γ - austenitic dendrite. Regarding austenitic filler material and cast structure, slightly lower threshold values of the stress concentration factor should be expected when cracks grow in the direction parallel to the columnar grain [22].

5. CONCLUSION

Based on the results, the following conclusions can be drawn:

- An effect of the relatively high hardness combined with a high impact energy achieved by using austenitic filler material allows increased resistance to crack initiation with a fatigue crack threshold ΔK_{th} = 10 MPa m$^{1/2}$, which results in better fatigue performance of the joint. Austenitic filler material showed a high threshold stress concentration factor. Microscopic testing showed,
- Direct transformation of γ - austenite into α' - martensite was ascertained in austenitic filler material AWS 307, with a 32 mJ/m2 fault energy.

REFERENCES

[1] L. Kuzmikova, J. Norrish, H. Li, M Callaghan, Research to establish a systematic approach to safe welding procedure development using austenitic filler material for fabrication of high strength steel. *16th International Conference on the Joining of Materials*, 2011, pp.1-13.

[2] B. Savic, A. Cabrilo, Effect of Heat Input on the Ballistic Performance of Armor Steel Weldments. *Materials*, 14(13), 2021: 3617. https://doi.org/10.3390/ma14133617

[3] E. Ranjbarnodeh, H. Pouraliakbar, A.H. Kokabi, Finite Element Simulation of Carbide Precipitation in Austenitic Stainless Steel 304. *International Journal of Mechanics and Applications*, 2(6), 2012: 117-123. https://doi.org/10.5923/j.mechanics.20120206.03

[4] M.M. Alam, Z. Barsoum, P. Jonsén, A.F.H. Kaplan, H.Å, Häggblad, Influence of defects on fatigue crack propagation in laser hybrid welded eccentric fillet joint. *Engineering Fracture Mechanics*, 78(10), 2011: 2246-2258.

https://doi.org/10.1016/j.engfracmech.2011.04.011

[5] A. Cabrilo, A. Sedmak, Z. Burzic, S. Perkovic, Fracture mechanics and fatigue crack propagation in armor steel welds. *Engineering Failure Analysis,* 106, 2019: 104155. https://doi.org/10.1016/j.engfailanal.2019.104155

[6] H. Pouraliakbar, M. Hamedia, A.H. Kokabia, A. Nazari, Designing of CK45 Carbon Steel and AISI 304 Stainless Steel Dissimilar Welds. *Materials Research*, 17(1), 2014: 106-114.

[7] S. Yu, J. Yan, H. Li, R. Ding, A. Lall, A. Rabiei, P. Bowen, Fatigue crack growth resistance of the austenitic stainless steel Alloy 709 at elevated temperatures. *Journal of Materials Research and Technology*, 9(6), 2020: 12955-12969. https://doi.org/10.1016/j.jmrt.2020.09.050

[8] D.F. Martelo, A. Mateo, M.D. Chapetti, Crack closure and fatigue crack growth near threshold of a metastable austenitic stainless steel. *International Journal of Fatigue*, 77, 2015: 64-77. https://doi.org/10.1016/j.ijfatigue.2015.02.016

[9] M. Moallemi, A. Kermanpur, A. Najafizadeh, A. Rezaee, S.H. Baghbadorani, D.P. Nezhadfar, Deformation-induced martensitic transformation in a 201 austenitic steel: The synergy of stacking fault energy and chemical driving force. *Materials Science and Engineering: A,* 653, 2016: 147-152. https://doi.org/10.1016/j.msea.2015.12.006

[10] S. Allain, J.P. Chateau, O. Bouaziz, S. Migot, N. Guelton, Correlations between the calculated stacking fault energy and the plasticity mechanisms in Fe–Mn–C alloys. *Materials Science and Engineering: A*, 387-389, 2004: 158-162. https://doi.org/10.1016/j.msea.2004.01.059

[11] E. Polatidis, W.-N. Hsu, M. Šmíd, T. Panzner, S. Chakrabarty, P. Pant, H. Van Swygenhoven, Suppressed martensitic transformation under biaxial loading in low stacking fault energy metastable austenitic steels. *Scripta Materialia*, 147, 2018: 27-32. https://doi.org/10.1016/j.scriptamat.2017.12.026

[12] Z. Mei, J.W. Morris, Influence of deformation-induced martensite on fatigue crack propagation in 304-type steels. *Metallurgical Transactions A*, 21, 1990: 3137-3152. https://doi.org/10.1007/BF02647310

[13] A. Cabrilo, K. Geric, Weldability of High hardness armour steel. *Advanced Materials Research*, 1138, 2016, 79-84. https://doi.org/10.4028/www.scientific.net/AMR.1138.79

[14] A.H. Monazzah, H. Pouraliakbar, R. Bagheri, S.M.S. Reihani, Toughness behavior in roll-bonded laminates based on AA6061/SiCp composites. *Materials Science and Engineering: A*, 598, 2014: 162-173. https://doi.org/10.1016/j.msea.2014.01.014

[15] ASTM E647-08: Standard test method for measurement of fatigue crack growth rates. In Annual Book of ASTM Standards. *ASM International*, West Conshohocken, USA, 2004.

[16] R.L. Snyder, The Use of Reference Intensity Ratios in X-Ray Quantitative Analysis. *Powder Diffraction*, 7(4), 1992: 186-193. https://doi.org/10.1017/S0885715600018686

[17] J. Lu, L. Hultman, E. Holmström, K.H. Antonsson, M.Grehk, W. Li, L. Vitos, A. Golpayegani, Stacking fault energies in austenitic stainless steels. *Acta Materialia*, 111, 2016: 39-46. https://doi.org/10.1016/j.actamat.2016.03.042

[18] P. Haušild, V. Davydov, J. Drahokoupil, M. Landa, P. Pilvin, Characterization of strain-induced martensitic transformation in a metastable austenitic stainless steel. *Materials & Design*, 31(4), 2010: 1821-1827. https://doi.org/10.1016/j.matdes.2009.11.008

[19] F. Xiong, Y. Liu, Effect of stress-induced martensitic transformation on the crack tip stress-intensity factor in Ni–Mn–Ga shape memory alloy. *Acta Materialia*, 55(16), 2007: 5621-5629. https://doi.org/10.1016/j.actamat.2007.06.031

[20] M. Nakajima, M. Akita, Y. Uematsuc, K. Tokaji, Effect of strain-induced martensitic transformation on fatigue behavior of type 304 stainless steel. *Procedia Engineering*, 2(1), 2010: 323-330. https://doi.org/10.1016/j.proeng.2010.03.036

[21] M. Grujicic, S.G. Lai, P. Gumbsch, Atomistic simulation study of the effect of martensitic transformation volume change on crack-tip material evolution and fracture toughness. *Materials Science and Engineering A*, 231(1-2), 1997: 151-162. https://doi.org/10.1016/S0921-5093(97)00068-3

[22] Y.-B. Shang, H.-J. Shi, Z.-X. Wang, G.-D. Zhang, In-situ SEM study of short fatigue crack propagation behavior in a dissimilar metal welded joint of nuclear power plant. *Materials & Design*, 88, 2015: 598-609. http://dx.doi.org/10.1016/j.matdes.2015.08.090